

# Atomic Deuterium Maser\*

D. J. Wineland<sup>†‡</sup> and N. F. Ramsey

*Lyman Laboratory of Physics, Harvard University, Cambridge, Massachusetts 02138*

(Received 21 July 1971)

An atomic deuterium maser operating on hyperfine transitions was used to measure the ground-state hyperfine separation in deuterium. The result was  $\nu_0(D) = 327\,384\,352.5222(17)$  Hz where the hydrogen hyperfine frequency is assumed to be exactly 1420 405 751.768 Hz. The construction of the device is discussed and a theory of the deuterium maser is presented with special attention given to frequency shifts occurring in the output frequency. In addition, a possible shift of the deuteron Larmor frequency because of the earth's gravitational field was also investigated and found to be  $<10^{-4}$  Hz.

## I. INTRODUCTION

The work reported here was motivated by the desire to obtain a more accurate measurement of the ground-state hyperfine splitting  $\nu_0(D)$  in deuterium. Although a more accurate measurement does not provide a better check of the theoretical value of  $\nu_0(D)$ ,<sup>1</sup> it is important for other reasons. For instance, in the measurements of the  $g_J$  ratios in the hydrogen isotopes,<sup>2,3</sup>  $\nu_0(D)$  is a parameter that must be known accurately to interpret the data. Moreover, it was useful to investigate the use of the deuterium maser as a possible alternative to the hydrogen-maser primary-frequency standard.

The most precise previous measurements<sup>4-6</sup> of  $\nu_0(D)$  have been made in experiments where resonances in deuterium were detected by monitoring the electron polarization in another pumped alkali which could interact with deuterium atoms via spin-exchange collisions. The accuracy in these experiments is ultimately limited by spin-exchange frequency shifts (due to deuterium-deuterium collisions) which can only be roughly estimated. In the atomic deuterium maser (D maser) such spin-exchange shifts are present; however, as in the hydrogen maser (H maser),<sup>7</sup> they are easily accounted for.

## II. DEUTERIUM HYPERFINE STRUCTURE

For the problem of deuterium ground-state hyperfine structure, the Hamiltonian of interest can be written

$$H = ha\vec{I} \cdot \vec{J} - g_J\mu_B\vec{J} \cdot \vec{H}_0 - g_I\mu_B\vec{I} \cdot \vec{H}_0, \quad (2.1)$$

where  $\mu_B$  is the Bohr magneton,  $g_J$  and  $g_I$  are the electron and nuclear  $g$  factors in the atom (note that  $g_J \approx -2$ ),  $\vec{J}$  and  $\vec{I}$  are the electron and nuclear spins, and  $\vec{H}_0$  is the externally applied static magnetic field. The first term is the Fermi contact term for the hyperfine interaction and the last two terms represent the interaction of the electron's magnetic moment and that of the deuteron with the external magnetic field. For  $J = \frac{1}{2}$ , an exact ana-

lytical solution exists for this Hamiltonian and is called the Breit-Rabi formula.<sup>8</sup> The hyperfine energy levels as a function of magnetic field are illustrated in Fig. 1. They are generally designated by numbers since there does not exist a convenient spin representation for which the Hamiltonian is diagonal at all magnetic fields. At low field ( $x \ll 1$ ) the wave functions can be approximated by the  $|F, m_F\rangle$  eigenstates as shown.

Since the maser detects energy differences between levels, a more useful diagram is the representation of the frequencies of the various transitions vs magnetic field. Such a diagram, which includes the two transitions which are least sensitive to magnetic field at low fields, is given in Fig. 2. (A more complete diagram is given elsewhere.<sup>9</sup>) We note that the  $2 \leftrightarrow 6$  transition frequency goes through a minimum at about 30 mG; hence if the maser is operated on this transition at the "field-independent" point, the output frequency is quite insensitive to fluctuations or drifts in the applied magnetic field ( $\vec{H}_0$ ). This was done in practice and therefore field-stability requirements were greatly

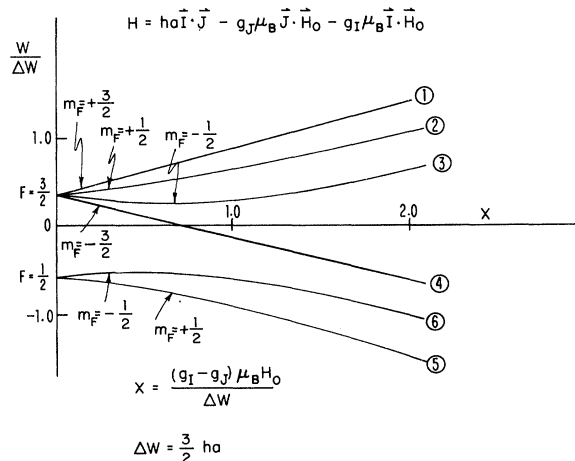


FIG. 1. Deuterium hyperfine energy levels as a function of magnetic field.

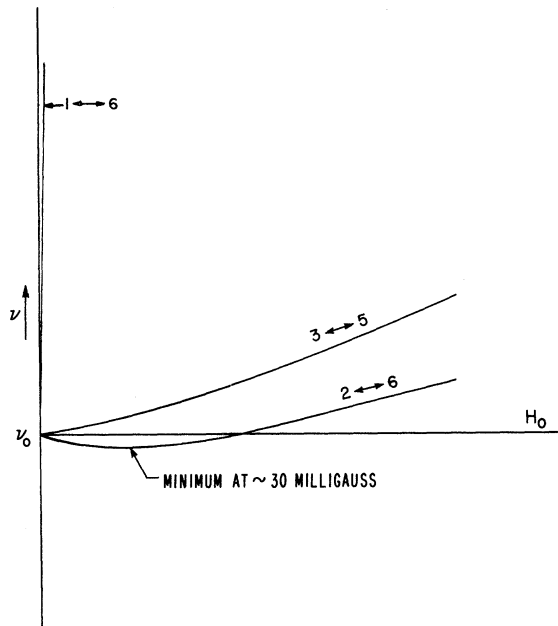


FIG. 2. Field dependence of the  $1 \leftrightarrow 6$ ,  $2 \leftrightarrow 6$ , and  $3 \leftrightarrow 5$  hyperfine transition frequencies.

simplified.

It should also be noted that the  $3 \leftrightarrow 6$   $\sigma$  transition frequency goes through a minimum at approximately 40 G but it was undesirable to operate the maser at these higher fields because (i) fractional-stability requirements on the solenoid supply would be more stringent, and (ii) field inhomogeneities would be larger at the higher fields causing sizeable inhomogeneity shifts (see Sec. VII B).

### III. APPARATUS

The D maser was constructed similarly to existing H masers.<sup>10-12</sup> It is illustrated schematically in Fig. 3. Deuterium atoms are created in and effuse out of an rf discharge bulb. A static hexapole magnet focuses the upper three hyperfine lev-

els into a beam while defocusing the lower three. This state-selected beam ( $\geq 10^{13}$  atoms/sec) then passes into a Teflon storage "bulb" which confines the atoms (for about 6 sec) in a constant phase microwave field defined by a circular-cylindrical cavity tuned to the hyperfine frequency and operating in the  $TE_{011}$  mode. When the cavity  $Q$  and atom fluxes are sufficiently large, self-sustained oscillations occur. The low, uniform magnetic fields required were supplied by a solenoid wound on the inside of a set of three concentric moly-permalloy magnetic shields.

In designing the maser, particular attention was paid to reducing systematic frequency shifts. This meant that optimum signal-to-noise conditions were not simultaneously achieved. However the resulting signal-to-noise ratio was adequate and did not limit the experiment. The most serious systematic shift is that due to the presence of neighboring transitions. [It is called  $\delta\nu_{53}(D)$  and is discussed in Sec. V E.] It is proportional to the square of the  $6 \leftrightarrow 2$  transition-frequency linewidth ( $\pi^{-1}\tau_2^{-1}$ ), and therefore minimizing this linewidth is important.

In practice, the limiting relaxation in this type of storage-bulb apparatus is due to atom collisions with the bulb surface. It is called wall relaxation and is designated  $T_{2w}^{-1}$ . For the D maser this relaxation could be estimated from studies done in the hydrogen maser.<sup>13-15</sup> It would be made smallest by constructing a multiple-region maser<sup>15</sup> with a large intermediate storage region, thereby reducing the atom collision rate with the wall surface. However, since it was desirable to utilize an existing vacuum system and magnetic shields,<sup>15,16</sup> a single cavity maser provided the smallest wall collision rate.

A second condition on linewidth is that it be partly due to spin exchange. When this is true, the linewidth can be varied by changing the atom density in the storage bulb (by changing the atom flux), which provides a convenient method for calculating spin exchange and cavity shifts in the output fre-

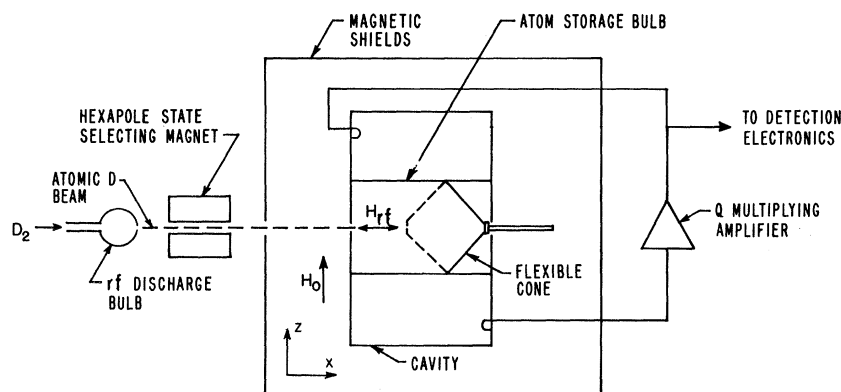


FIG. 3. Schematic diagram of the apparatus.

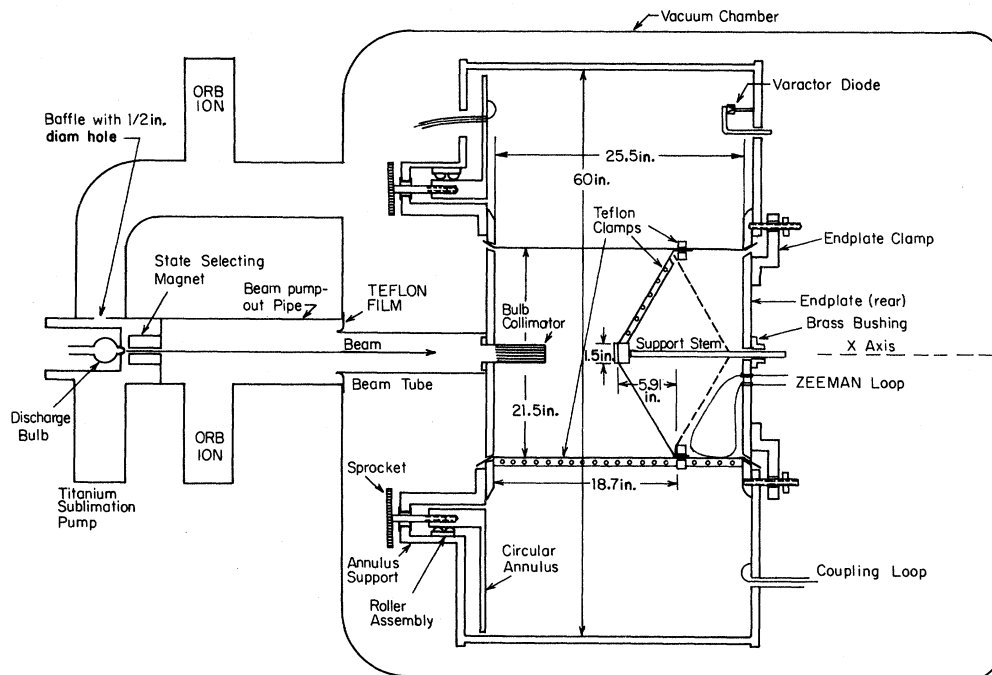


FIG. 4. Detailed schematic of cavity and vacuum chamber.

quency.<sup>11</sup> We would like all other relaxation processes to be comparatively small. For instance, we would like the relaxation due to escape from the bulb ( $T_b^{-1}$ ) to be such that  $T_b \gg \tau_2$ .

Therefore, if  $T_{2w}$  is known, then  $T_b$  should be chosen such that  $T_b \gg T_{2w}$ . With this value of  $T_b$  the atom flux level is governed by the requirement that spin-exchange relaxation  $T_{2SE}^{-1}$  be comparable to wall relaxation. Now that the flux levels are specified we must have a high enough cavity  $Q$  value in order to achieve oscillation. [More generally, the quality parameter  $m$  must be small enough (see Sec. VA).]

#### A. Storage Bulb and Cavity

In practice the above design principles could not be strictly followed. If we make  $T_b$  arbitrarily large, then an arbitrarily small flux is required in order to make  $T_{2SE}$  comparable to  $T_{2w}$ . This means that only a very small power output is available from the atoms and therefore an arbitrarily high cavity  $Q$  is needed to sustain oscillation. For reasons discussed below, this is undesirable and therefore  $T_b$  was chosen to be on the order of  $T_{2w}$  and  $T_{2SE}$ .

Even with the highest obtainable fluxes, oscillation could not be obtained with the natural  $Q$  of the cavity ( $Q_{c0}$ ). (In practice  $Q_{c0} \approx 0.8 \times 10^5$  while the maximum theoretical value is  $Q_{c0} \approx 1.0 \times 10^5$  for the type of cavity used.) Therefore an external feedback amplifier (Fig. 3) was used to compensate partially resistive losses in the cavity and thereby

raise the  $Q$  to a large enough value to achieve oscillation. Unfortunately this scheme has the effect of adding unwanted noise to the maser oscillation and increasing frequency drifts due to cavity pulling. In addition, the system is critically dependent on amplifier gain stability; if the gain becomes too high, the cavity plus amplifier system will self-oscillate. This puts practical limits on the maximum obtainable  $Q$ ; in this experiment stable  $Q$ 's of  $3 \times 10^6$  could be obtained; however, typical operating  $Q$ 's were chosen to be  $\approx 4 \times 10^5$ .

It should be noted that the main difficulties with the "Q-multiplied" scheme can be avoided if one uses a two-cavity scheme with external amplification between the cavities. In this arrangement frequency shifts caused by the cavities should be the same as for the isolated cavities regardless of the amplification between them.<sup>15</sup> Moreover, since the feedback "loop" is completed by the atoms, the cavity-amplifier system is stable for all gain values.

The most difficult problems encountered in the construction of the D-maser cavity and storage bulb were caused by the required large size of these pieces. (Since the D maser was made similarly to existing H masers, the dimensions of the apparatus scale approximately as the ratio of the wavelengths.) It would be desirable to construct the cavity of a low thermal-expansion-coefficient material but this was prohibitively expensive and impractical. Therefore the all aluminum cavity shown in Fig. 4 was constructed. A circular annulus forms one

end of the cavity and by moving on rollers in the  $\pm x$  direction provides the coarse tuning for the cavity. This movement is controlled by four rods which are threaded into the annulus but pass through the "annulus support" on Teflon bushings. Movement of these rods in the  $x$  direction is constrained relative to the annulus support, but by turning them one way or the other, the annulus can be moved back and forth. The turning of these rods is synchronized by attaching sprockets to the ends of the rods external to the cavity and connecting them with a chain. Finally, the motion of the annulus can be accomplished external to the vacuum chamber by connecting a rotary vacuum feedthrough<sup>17</sup> to one of the sprockets. Fine tuning of the cavity is provided by a voltage variable reactance (in the form of a varactor) coupled into the cavity.<sup>15</sup>

In order to isolate thermally the cavity from the vacuum chamber and therefore reduce temperature drifts, the direct thermal contacts between the cavity and vacuum chamber were kept at a minimum. The cavity rested on four small Teflon blocks which were attached to an aluminum dolly whose wheels were mounted on Teflon bushings. The "beam tube" was connected to the "pump-out pipe" with a thin sheet of Teflon film. The vacuum chamber was internal to the structure containing the magnetic shields and thermal insulation.<sup>15</sup> However, it was not temperature controlled. With this arrangement, typical cavity-drift rates were  $\leq 2$  Hz/min; moreover, it was determined that frequency drifts were primarily due to the cavity and not the  $Q$ -multiplication electronics.

Because the cavity was quite opaque to radiation at the Zeeman frequency ( $\approx 29$  kHz), the Zeeman-transition-inducing loop (used to monitor the magnetic field) was placed inside the cavity. This does not affect the cavity mode of interest provided that the loop does not couple to this mode.

For the atom storage bulb, similar problems due to large size were encountered. It was impractical and prohibitively expensive to make a storage bulb of glass or quartz as is done for the H maser.<sup>11</sup> Therefore a multipiece storage region of Teflon film<sup>18</sup> was constructed (Fig. 4). The essential features of the bulb are the outer cylinder of Teflon film, the aluminum endplate coated with Teflon, the two-position Teflon cone used to vary the bulb volume and therefore determine the "wall" frequency shift (see Sec. V B), and the Teflon collimator used to increase the bulb lifetime. The outer cylinder was made of one sheet of 20-mil film. A seam was made along a generator of the cylinder by use of a solid Teflon clamp. The flexible cone was made of a flat sheet of 2-mil film and had one seam made like the one for the outer cylinder; it was attached to the outer cylinder by a similar clamping arrangement. The bulb was held in the

small-volume position (solid line in Fig. 4) or the large-volume position (dashed line in Fig. 4) by a copper stem attached to the cone with a circular Teflon plug and attached to the rear of the cavity with a brass bushing.

The front endplate, which formed the front part of the bulb, and the rear endplate, both of which served as part of the endplates for the cavity, were made of aluminum and coated commercially<sup>19</sup> with at 1.5 mil thickness of FEP film. The edges of these plates and the corresponding parts of the cavity were cut at slight angles (greatly exaggerated in Fig. 4) so that a tight seal could be made between the outer cylinder and cavity endplates when these endplates were clamped down.

The collimator was made of many parallel sections of Teflon tubing (FEP-shrinkable wire cover). These tubes were held in a single tube of FEP-shrinkable roll cover which was mounted to the entrance aperture of the bulb.

Cleaning the interior of the bulb was provided by washing with Freon and good quality trichlorethylene. Acid was not used mainly because of the difficulty in handling the bulb, which would retain its shape only when held in the cavity. When under vacuum, only mild baking ( $< 80^\circ\text{C}$ ) could be used or else the Teflon would distort and shrink.

With the above-described bulb (with the mean free path for wall collisions at small volume  $\lambda_{sv} \approx 11.7$  in.) the expected wall relaxation rate based on studies done in the hydrogen maser with DuPont FEP-120 Teflon film coated onto quartz storage bulbs<sup>13,14</sup> would be  $1.6 < T_{2w} < 12$  sec.<sup>20</sup> In order to keep cavity  $Q$  at a reasonable level and still achieve oscillation without excessive spin-exchange relaxation, the storage times were chosen such that  $T_{b_{sv}} \approx 5.9$  sec,  $T_{b_{lv}} \approx 7.5$  sec, where the subscripts refer to the small- and large-volume configurations of the bulb.

#### B. Source and Vacuum System

The atom source and focusing magnet are similar to those described elsewhere.<sup>11</sup> The essential features of the vacuum system have also been described elsewhere.<sup>15,16</sup> In order to reduce the pumping requirements of the existing orb-ion pumps,<sup>15</sup> a glass-fused capillary array with a  $\kappa$  factor of approximately 16 was added to the source bulb (Bendix Mosaics, Sturbridge, Mass.). In addition, a baffle and extra pump (Granville-Phillips titanium sublimation pump) were added to the source chamber as indicated in Fig. 4. Pressures were measured with Varian UHV series gauges placed in recesses near the pump openings. With the source turned off the pressure measured at the lower orb ion was typically  $2 \times 10^{-8}$  Torr. (This reading is the apparent reading normalized to  $\text{N}_2$  gas;  $\text{H}_2$  gives a reading which is high by a factor

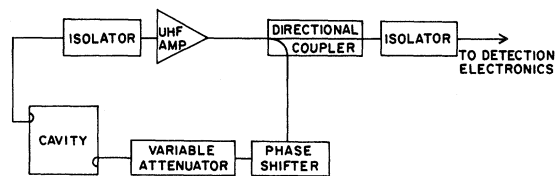


FIG. 5. Block diagram of the  $Q$ -multiplication scheme.

of 2.) With an atom flux of  $(2 \pm 1) \times 10^{13} \text{ sec}^{-1}$ , the measured pressure at the lower orb ion is  $3 \times 10^{-8}$  Torr. At this flux and at  $T_b = 6 \text{ sec}$  the calculated bulb pressure is  $2 \times 10^{-8}$  Torr.

#### C. Magnetic Shields and Solenoid

The magnetic shields surrounding the cavity and main vacuum chamber have been discussed elsewhere.<sup>15,16</sup> A solenoid was wound inside but as close as possible to the innermost shield. The spacing between windings was  $\approx 1 \text{ in.}$ , and a current of  $\approx 60 \text{ mA}$  produced the required operating field of  $\approx 30 \text{ mG}$  in a direction perpendicular to the cavity axis and normal to the earth's surface. Linewidths of the Zeeman transitions ( $\nu_{\pi} \approx \mu_B g_J H_0 / 3\hbar$ ) were primarily attributed to magnetic field inhomogeneities; typically they were  $\approx 3 \text{ Hz}$ . Assuming a model for the inhomogeneities one can estimate their magnitude.<sup>10</sup>

#### D. Electronics

$Q$  multiplication of the cavity was accomplished in a straightforward manner and is quite similar to schemes used by other authors.<sup>21</sup> The block diagram in Fig. 5 illustrates the technique and a simple analysis of this system is given in the Appendix.

The detection electronics compared the output frequencies of the deuterium and hydrogen masers; therefore it primarily consisted of amplifiers, mixers, and filters. The essential elements of the comparison electronics are illustrated in Fig. 6. The crystal oscillator is locked to the H maser as shown in the left-hand side of the diagram. Both the frequency provided by "synthesizer 2" and the time base for the counter can be expressed as a function of  $\nu(H)$ ; therefore the counted signal ( $\nu_{\text{beat}}$ ) gives a comparison of  $\nu(D)$  with respect to  $\nu(H)$ . In practice the "phase detector" and "mixer" consisted of several mixers, filters, and amplifiers,<sup>22</sup> and the crystal was offset about 5.3 parts in  $10^8$  in order to simplify synthesizer requirements.

To observe radiative decay times in the maser, a pulsing scheme similar to that described by Berg<sup>23</sup> was used. Typically, pulse lengths were 0.1 sec in duration and the pulsing amplitude was adjusted to obtain  $\approx \frac{1}{2} \pi$  spin flips. At flux levels used for oscillation,  $S/N$  on the initial decay amplitude was  $\approx 20/1$ .

#### IV. THEORY

Section II discussed the static problem of deuterium hyperfine structure; the Breit-Rabi formula yielded the energies of the various levels in a static magnetic field  $\vec{H}_0$ . Now we discuss the dynamical problem of the maser; therefore we must include the effects of the oscillating electromagnetic field, collisions, etc. Experimentally, the frequency of the radiation in the maser cavity  $\nu(D)$  is measured. Therefore we need expressions which relate the observed frequency  $\nu(D)$  to  $\nu_0(D)$ . To do this, it is convenient to break the problem into two parts. That is, we find (i) an equation that relates the radiation in the maser to both the cavity and magnetization due to the atoms and (ii) equations that relate the magnetization to the atoms. (Specifically we will relate the magnetization to the density matrix representing the atoms.) These equations can then be solved to give an expression for the power emitted and the frequency of oscillation in terms of measurable or calculable quantities. Specifically, the expression for the output frequency can be written in terms of the atomic and cavity frequencies and suggests the experimental technique for determining  $\nu_0(D)$ . We first discuss the problem of the atoms interacting with their environment and obtain an expression for the magnetization; later we relate the radiation to its environment (cavity and magnetization).

For a description of the atoms it is useful to use the density-matrix approach.<sup>24</sup> This method has previously been used to describe the hydrogen maser<sup>5,25</sup> and yields all the available information when the motions of individual atoms in an ensemble are not known. Following Crampton<sup>5</sup> we write the equation for the rate of change of the deuterium density matrix  $\rho(D)$  as

$$\frac{d}{dt} \rho(D) = \left( \frac{d}{dt} \rho(D) \right)_{SE} + \left( \frac{d}{dt} \rho(D) \right)_F + \left( \frac{d}{dt} \rho(D) \right)_{RAD} + \left( \frac{d}{dt} \rho(D) \right)_{OR}, \quad (4.1)$$

where the subscripts stand for spin-exchange colli-

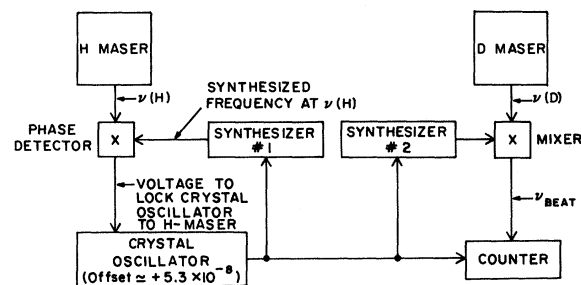


FIG. 6. Block diagram of the frequency comparison electronics.

TABLE I. Factors multiplying collision rates for deuterium spin exchange.

$$\begin{aligned}
A(1) &= \frac{1}{2}(1-P)D_{11} - \frac{1}{6}(1+P)(D_{22} + 2D_{55}) \\
A(2) &= -\frac{1}{6}(1-P)(D_{11} - D_{22}) - \frac{1}{9}(1+P)(2D_{33} + D_{66}) + \frac{1}{9}(5D_{22} - 2D_{55}) \\
A(3) &= -\frac{1}{9}(1-P)(2D_{22} + D_{55}) + \frac{1}{6}(1+P)(D_{33} - D_{44}) + \frac{1}{9}(5D_{33} - 2D_{66}) \\
A(4) &= -\frac{1}{6}(1-P)(D_{33} + 2D_{66}) + \frac{1}{2}(1+P)D_{44} \\
A(5) &= -\frac{1}{6}(1-P)D_{11} - \frac{1}{18}(1+P)(2D_{33} - 3D_{55} + D_{66}) - \frac{1}{9}(2D_{22} - 5D_{55}) \\
A(6) &= -\frac{1}{18}(1-P)(2D_{22} + D_{55}) - \frac{2}{9}D_{33} - \frac{1}{3}(1+P)D_{44} + \left(\frac{4}{18} - \frac{1}{6}P\right)D_{66} \\
A(7) &= \frac{1}{27}(15D_{11} + 14D_{22} + 17D_{33} + 24D_{44} + 19D_{55} + 16D_{66}) \\
A(8) &= \frac{1}{27}(24D_{11} + 17D_{22} + 14D_{33} + 15D_{44} + 16D_{55} + 19D_{66}) \\
P = 2\langle J_{\mathbf{r}} \rangle &= D_{11} + \frac{1}{3}D_{22} - \frac{1}{3}D_{33} - D_{44} - \frac{1}{3}D_{55} + \frac{1}{3}D_{66}
\end{aligned}$$

sions (SE), flow contributions (F), radiation and "free  $P$  recession" (RAD), and other relaxation not included in the first three terms (OR). We will eventually be interested in the conditions of steady state; therefore, for the left-hand side of Eq. (4.1) we will set  $D_{ii} = 0$  and  $D_{ij} \propto e^{i2\pi\nu(D)t}$ , where  $D_{ij}$  is an individual element of  $\rho(D)$ .<sup>5</sup> Since the problem is similar to that treated for the H maser,<sup>5,25</sup> development and discussion of the equations apply only to the particular example of the deuterium maser.

#### A. Spin Exchange

Crampton,<sup>5,26</sup> has derived the contribution due to spin exchange. It should be noted that only the main terms are discussed here; small corrections due to nuclear identity, for example, are discussed in Sec. VII B. The diagonal terms are

$$\dot{D}_{ii} = -A(i)/T_{DD}, \quad i = (1, 6) \quad (4.2)$$

where

$$T_{DD}^{-1} = n(D)\langle V_{\mathbf{r}\mathbf{e}1} \sigma_{SF}(D, D) \rangle_k$$

or

$$T_{DD}^{-1} = n(D)\langle (\pi\hbar/\mu k) \sum_{l=0}^{\infty} (2l+1) \sin^2(\delta_l^3 - \delta_l^1) \rangle_k.$$

$T_{DD}^{-1}$  is the collision rate and  $n(D)$  is the deuterium density. The product of the relative velocity of the atoms  $V_{\mathbf{r}\mathbf{e}1}$  and "spin-flip" cross section  $\sigma_{SF}(D, D)$  can be written in terms of phase shifts for the triplet and singlet wave functions for the different angular momenta during the collision; the average is over the thermal velocity distribution. The  $A(i)$  are given in Table I. [Note that the equation for  $(\dot{D}_{66})_{SE}$  given in Ref. 5 is incorrect.]

The off-diagonal elements of interest are  $D_{62}$  and  $D_{53}$ . We have

$$(\dot{D}_{62})_{SE} = [-A(7)/T_{DD}]D_{62} + i\Delta\omega_{62}(SE)D_{62} \quad (4.3)$$

and

$$(\dot{D}_{53})_{SE} = [-A(8)/T_{DD}]D_{53} + i\Delta\omega_{53}(SE)D_{53}, \quad (4.4)$$

where

$$\Delta\omega_{62}(SE) \equiv -[\kappa_{DD}/9T_{DD}](D_{22} - D_{66}),$$

$$\Delta\omega_{53}(SE) \equiv -[\kappa_{DD}/9T_{DD}](D_{33} - D_{55}),$$

$$\kappa_{DD}/T_{DD} \equiv n(D)\langle V_{\mathbf{r}\mathbf{e}1} k(D, D) \rangle$$

$$= n(D) \left\langle \left( \pi\hbar/2\mu k \right) \sum_{l=0}^{\infty} (2l+1) \sin 2(\delta_l^3 - \delta_l^1) \right\rangle_k.$$

$\kappa_{DD}$  is called the frequency-shift parameter.<sup>5</sup>

#### B. Flow

The "flow" contributions to Eq. (4.1) can be written<sup>25</sup>

$$(\dot{D}_{ii})_F = (1/T_b)(C_{ii} - D_{ii}), \quad i = (1, 6) \quad (4.5)$$

$$(\dot{D}_{ij})_F = -(1/T_b)D_{ij}, \quad i \neq j = (1, 6)$$

where  $T_b^{-1}$  is the geometrical relaxation rate out of the bulb, and the  $C_{ii}$  are parameters which specify the degree of state selection in the beam which enters the storage bulb. For example, if the state-selecting magnet is working "ideally" (i.e., selecting the upper three hyperfine levels and rejecting the lower three), then  $C_{11} = C_{22} = C_{33} = \frac{1}{3}$  and  $C_{44} = C_{55} = C_{66} = 0$ .

#### C. Other Relaxation

Contributions by other relaxation mechanisms (e.g., wall relaxation, Majorana flops, magnetic-field-inhomogeneity dephasing) are written

$$(\dot{D}_{ii})_{OR} = (1/T_1)\left(\frac{1}{6} - D_{ii}\right), \quad i = (1, 6) \quad (4.6)$$

$$(\dot{D}_{ij})_{OR} = -(1/T_2)D_{ij}, \quad i \neq j = (1, 6).$$

Clearly this is only an approximation. For instance, Majorana relaxation rates are different for different levels. However, since this is not a dominant relaxation process, its exact description is not as important. More significantly, frequency shifts caused by the above effects are either directly measurable (e.g., wall shift) or negligible.

#### D. Radiation

Contributions to Eq. (4.1) due to radiation arise when an oscillating electromagnetic field connects the various levels of the system. Here the D maser exhibits a small but important difference compared with the H maser. The reason is that while the radiation in the D maser is predominantly due to the  $6 \leftrightarrow 2$  transition, there is a slight contribution by the nearby  $3 \leftrightarrow 5$  transition.<sup>27</sup> At the desired operating field ( $\approx 30$  mG) these two transitions are separated by only  $\approx 40$  Hz, and therefore there is a small but significant overlap of the lines. This gives rise to a frequency shift derived in Sec. V E.

Strictly speaking the derivation of  $(d/dt)\rho(D)_{RAD}$  should be made by treating the field quantum me-

chanically,<sup>28,29</sup> but for our purposes a classical treatment is sufficient. Therefore we wish to add to the Hamiltonian of Eq. (2.1) the term

$$V = -\mu_B(g_J \vec{J} + g_I \vec{I}) \cdot \vec{H}_1 \cos \omega t, \quad (4.7)$$

where  $\vec{H}_1$  is perpendicular to  $\vec{H}_0$ . (The 6  $\rightarrow$  2 transition is a  $\pi$  transition.) Choosing  $\vec{H}_1 = H_1 \hat{i}$ , we have  $V \approx \mu_B H_1 J_x e^{i\omega t}$ , where we have neglected the anti-rotating component of the field and the coupling to the nuclear moment. The latter approximation causes no frequency shift and makes a negligible correction to the power emitted by the atoms. Most straightforwardly,  $(d/dt)\rho(\mathbf{D})_{\text{RAD}}$  can be derived from the equation

$$\frac{d}{dt} \rho(\mathbf{D}) = \frac{i}{\hbar} [H', \rho(\mathbf{D})], \quad (4.8)$$

where  $H' = H + V$  and  $H$  is the Hamiltonian of Eq. (2.1). The only significant contributions to Eq. (4.1) from Eq. (4.8) are the terms  $(\dot{D}_{ij})_{\text{RAD}}$ , where  $i$  and  $j$  refer to levels for which there is a significant transition probability because of radiation. If we include all the terms of Eq. (4.8) in Eq. (4.1) then for steady-state conditions we obtain a set of simultaneous nonlinear (because of spin exchange) algebraic equations which must be solved. For steady-state conditions the solution for the off-diagonal elements can be written in the form  $D_{ij} = (\alpha_{ij} + i\beta_{ij})e^{i\omega t}$ , where  $\alpha_{ij}$  and  $\beta_{ij}$  are real and  $\omega$  is the angular frequency of the radiation. When  $\omega$  is nearly equal to the angular frequency for the 6  $\rightarrow$  2 transition, then  $\alpha_{62}$  and  $\beta_{62}$  would be significantly large and, for all other  $i, j$ ,

$$\alpha_{ij} = \frac{1}{2} x f_{ij} (\omega_{ij} - \omega_{62})^{-1}, \quad (4.9)$$

$$\beta_{ij} = \alpha_{ij} (\omega_{ij} - \omega_{62})^{-1} \tau_{2ij}^{-2},$$

where

$$x \equiv (2\mu_B H_1 / \hbar) \langle 6 | J_x | 2 \rangle, \quad |f_{ij}| \lesssim 1$$

and  $\omega_{ij}$  is the resonant frequency of the atoms on the  $i \rightarrow j$  transition and can be written as  $2\pi\nu_0(\mathbf{D})$  plus corrections due to wall shift, magnetic field shift, and second-order Doppler shift [see Eq. (5.4)]. Therefore the only other significant contributions from Eq. (4.8) to Eq. (4.1) come from the 3  $\rightarrow$  5 transition. For these two transitions of interest, we have

$$(\dot{D}_{22})_{\text{RAD}} = x\beta_{62}, \quad (4.10a)$$

$$(\dot{D}_{66})_{\text{RAD}} = -x\beta_{62}, \quad (4.10b)$$

$$(\dot{D}_{62})_{\text{RAD}} = i\omega_{62} D_{62} - i\frac{1}{2} x (D_{22} - D_{66}) e^{i\omega t}, \quad (4.10c)$$

$$(\dot{D}_{33})_{\text{RAD}} = -x\beta_{53}, \quad (4.10d)$$

$$(\dot{D}_{55})_{\text{RAD}} = x\beta_{53}, \quad (4.10e)$$

$$(\dot{D}_{53})_{\text{RAD}} = i\omega_{53} D_{53} + i\frac{1}{2} x (D_{53} - D_{55}) e^{i\omega t}. \quad (4.10f)$$

### E. Expression for Magnetization

We now obtain an expression for the atomic magnetization in terms of the density matrix. We are interested in the average over the bulb of the  $x$  component of the magnetization; for a single atom the relevant operator is  $\mu_x = g_J \mu_B J_x + g_I \mu_B I_x$ . The total magnetization can be written

$$M_{x\text{TOT}} \equiv \langle M_x \rangle_b e^{i\omega t} + \langle M_x \rangle_b^* e^{-i\omega t} = (N/V_b) \langle \mu_x \rangle_b, \quad (4.11)$$

where  $N$  is the total number of deuterium atoms in the bulb and  $V_b$  is the bulb volume. Neglecting the nuclear moment we obtain

$$\begin{aligned} \langle \mu_x \rangle_b &= g_J \mu_B \\ &\times [\langle 6 | J_x | 2 \rangle (D_{62} + D_{62}^*) + \langle 5 | J_x | 3 \rangle (D_{53} + D_{53}^*)] \end{aligned} \quad (4.12)$$

and therefore

$$\begin{aligned} \langle M_x \rangle_b &= -(IT_b/V_b)(2\mu_B) \\ &\times [(\alpha_{62} + i\beta_{62}) \langle 6 | J_x | 2 \rangle + (\alpha_{53} + i\beta_{53}) \langle 5 | J_x | 3 \rangle], \end{aligned} \quad (4.13)$$

where  $I$  is the total atom flux.

### F. Equation of Motion for Field; Slater Equation

Previously<sup>10</sup> the problem of an equation of motion for the field has been solved by using a result derived by Slater<sup>30</sup> that relates the magnetization in a microwave cavity to the radiation. An equally rigorous but perhaps more transparent approach to the problem is given here. In this derivation the phases of the magnetization, oscillating field, and currents are easily accounted for<sup>31</sup>; however it is essentially the same as the one given by Slater. As before we treat the field classically.

The derivation given here relies on the assumption that near resonance for a particular cavity mode we can approximate the microwave cavity, associated coupling loop, and output line (terminated by an impedance  $Z_l$ ) by a series LRC circuit.<sup>32</sup> The analogy is especially clear if we consider a reentrant-type cavity where the electric and magnetic field energies are confined primarily to different regions of the cavity. Since the atoms interact only with the oscillating magnetic field  $H_1$ , we assume that inside the inductance  $L$  there exists a region of magnetization  $M$ . Thus, the model of the maser can be given as in Fig. 7. A coupling parameter  $\beta$  is defined in terms of a load matched to the line; that is, if  $Z_l = Z_0$ , which is the characteristic impedance of the line, then  $n^2 Z_0 / R = \beta$ . (For simplicity we assume  $Z_l = Z_0$  throughout the following.)

Faraday's law of induction yields the voltage across the inductor

$$V = K \frac{d}{dt} \langle B_x \rangle_b, \quad (4.14)$$

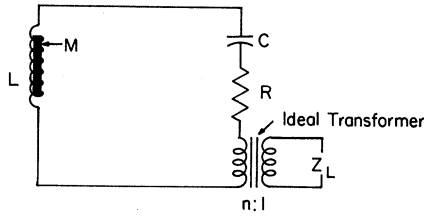


FIG. 7. Circuit analog of the maser.

where  $K$  is a real constant containing geometrical and units factors and  $\langle B_x \rangle_b$  is the average oscillating magnetic-field amplitude in the  $x$  direction over the region of the magnetization (e.g., bulb volume). We can also write

$$V = K \frac{d}{dt} [\langle H_x \rangle_b + 4\pi\eta' \langle M_x \rangle_b], \quad (4.15)$$

where  $\eta'$  is the usual filling factor<sup>10</sup>

$$\eta' = \eta \frac{V_b}{V_c} = \frac{\langle H_x \rangle_b^2 V_b}{\langle H^2 \rangle_c V_c},$$

$V_b$  is the bulb volume, and  $V_c$  is the cavity volume. Ampère's law says

$$\langle H_x \rangle_b = K' I, \quad (4.16)$$

where  $K'$  is a real constant containing geometrical and unit factors and  $I$  is the current. Using Eq. (4.16) in Eq. (4.15) and assuming that the magnetization is zero, we obtain

$$KK' = L. \quad (4.17)$$

Summing the voltage around the circuit we obtain with the help of Eqs. (4.14) through (4.17)

$$L \left( \frac{d}{dt} \langle H_x \rangle_b + 4\pi\eta' \frac{d}{dt} \langle M_x \rangle_b \right) + R(1 + \beta) \langle H_x \rangle_b + \frac{1}{C} \int \langle H_x \rangle_b dt = 0. \quad (4.18)$$

Taking the derivative of this equation with respect to time we obtain

$$\frac{d^2}{dt^2} \langle H_x \rangle_b + \frac{\omega_c}{Q_L} \frac{d}{dt} \langle H_x \rangle_b + \omega_c^2 \langle H_x \rangle_b = -4\pi\eta' \frac{d}{dt} \langle M_x \rangle_b, \quad (4.19)$$

where

$$\omega_c^2 = (LC)^{-1}, \quad Q_L = \frac{Q_c}{1 + \beta}, \quad Q_c = \frac{\omega_c L}{R}.$$

This can be taken as the classical equation for the field in a cavity near resonance. If we assume that the field and magnetization vary as  $e^{i\omega t}$ , then using the definition of  $\eta'$  we can rewrite Eq. (4.18) in the form

$$\frac{1}{Q_L} + i \left( \frac{\omega}{\omega_c} - \frac{\omega_c}{\omega} \right) + 4\pi i \frac{\langle M_x \rangle_b \langle H_x \rangle_b V_b}{\langle H^2 \rangle_c V_c} = 0. \quad (4.20)$$

This is the result obtained by directly applying the Slater equation<sup>30</sup> to the problem of the maser.<sup>10</sup>

#### G. Solutions to Equations of Motion; Oscillation Conditions

We now have the necessary equations [(4.1) and (4.20)] to solve for the output power and frequency of the maser. We first solve for the power and establish the conditions that must be met to achieve oscillation.

For this problem we need the real part of Eq. (4.20) which merely states that the power radiated by the atoms is equal to the power absorbed by the cavity. We assume that the power radiated by the 3 → 5 transition is negligible; that is, we assume that the contributions (4.10d) and (4.20e) can be neglected in Eq. (4.1) and that  $\alpha_{53} = \beta_{53} = 0$  in Eq. (4.13). One can work the problem without these assumptions but the difference in power output is negligible. The real part of Eq. (4.20) yields

$$x = -6(I/I_0) T_b \beta_{62}, \quad (4.21)$$

where we have defined

$$I_0 = \frac{3\hbar V_b}{4\pi\mu_B^2 Q (2\langle 6 | J_x | 2 \rangle)^2 \eta' T_t^2},$$

and, following Ref. 11,

$$1/T_t^2 = (1/T_1 + 1/T_b)(1/T_2 + 1/T_b).$$

Next we write the expression for  $\dot{D}_{62}$ . We have from Eqs. (4.1), (4.3), (4.5), (4.6), and (4.10) that

$$\dot{D}_{62} = -(1/\tau_2) D_{62} + i\omega'_{62} D_{62} - i\frac{1}{2} x (D_{22} - D_{66}) e^{i\omega t}, \quad (4.22)$$

where

$$\omega'_{62} = \omega_{62} + \Delta\omega_{62}(\text{SE})$$

and

$$\frac{1}{\tau_2} = \frac{1}{\tau_{262}} = \frac{1}{T_b} + \frac{1}{T_2} + \frac{1}{T_{2SE}},$$

$$\frac{1}{T_{2SE}} = \frac{A(7)}{T_{DD}}.$$

For steady-state conditions we assume  $D_{62} = (\alpha_{62} + i\beta_{62}) e^{i\omega t}$ . Therefore Eq. (4.22) yields

$$\alpha_{62} = \tau_2 (\omega - \omega'_{62}) \beta_{62} \quad (4.23)$$

and

$$(\omega - \omega'_{62}) \alpha_{62} + (\beta_{62}/\tau_2) + \frac{1}{2} x (D_{22} - D_{66}) = 0. \quad (4.24)$$

Although they are not needed here, we write the corresponding equations for the 3 → 5 transition. We have

$$\alpha_{53} = \tau_2 (\omega - \omega'_{53}) \beta_{53}, \quad (4.25)$$

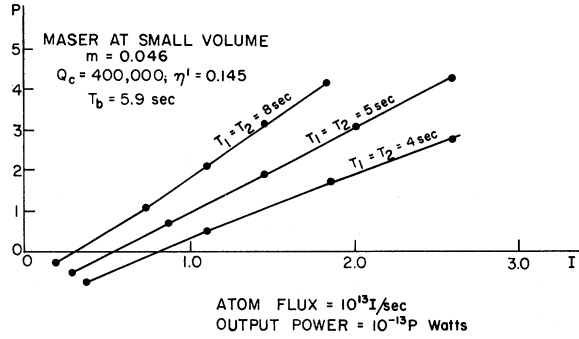


FIG. 8. Theoretical plots of maser power vs atom flux.

$$(\omega - \omega'_{53})\alpha_{53} + (\beta_{53}/\tau'_2) - \frac{1}{2}\chi(D_{33} - D_{55}) = 0, \quad (4.26)$$

where

$$\omega'_{53} = \omega_{53} + \Delta\omega_{53}(\text{SE}),$$

$$\frac{1}{\tau'_2} \equiv \frac{1}{\tau_{253}} = \frac{1}{T_b} + \frac{1}{T_2} + \frac{A(8)}{T_{DD}}.$$

Combining Eqs. (4.21)–(4.24), and noting that  $(\omega - \omega'_{62}) \ll \tau_2$  when the maser is oscillating, we obtain

$$(D_{22} - D_{66}) - \frac{T_i^2}{3(I/I_0)T_b\tau_2} = 0. \quad (4.27)$$

If we define  $P_0 \equiv \frac{1}{8}\hbar\omega I_0$  and note that the power radiated by the atoms can be expressed as  $P = -N\hbar\omega \times (\dot{D}_{22})_{\text{RAD}}$ , then with the help of Eq. (4.10a) we can write

$$(\dot{D}_{22})_{\text{RAD}} = -\frac{P/P_0}{6T_b(I/I_0)}.$$

Therefore the diagonal equations in Eq. (4.1) can be written

$$\dot{D}_{ii} = -\frac{A(i)}{T_{DD}} + \frac{1}{T_b}(C_{ii} - D_{ii}) + \frac{1}{T_1}\left(\frac{1}{8} - D_{ii}\right) + \delta_i \frac{(P/P_0)}{6T_b(I/I_0)}, \quad i = (1, 6) \quad (4.28)$$

where

$$\delta_6 = -\delta_2 = 1 \quad \text{and} \quad \delta_1 = \delta_3 = \delta_4 = \delta_5 = 0.$$

Equations (4.27) and (4.28) (with the requirement that  $\dot{D}_{ii} = 0$  for all  $i$ ) form a set of seven simultaneous nonlinear algebraic equations in seven unknowns [ $D_{ii}$ ,  $i = (1, 6)$  and  $P/P_0$ ]. Unfortunately, a simple analytic solution does not exist as in the case of the hydrogen  $\sigma$  maser.<sup>11,33</sup> For the D-maser problem an exact solution is not necessary from the standpoint of power considerations. However, it was desirable to make an exact solution in order to study the pulling by the nearby  $3 \rightarrow 5$  transition. Therefore a computer program was used; a typical plot

of power vs flux using measured input parameters ( $m$ ,  $T_b$ ,  $T_1$ ,  $T_2$ ,  $\tau_2$ ) is shown in Fig. 8. [ $m$  is defined as

$$\frac{\langle V_{\text{rel}} \sigma_{\text{SF}}(D, D) \rangle \hbar}{\pi \mu_B^2 \eta' Q}$$

and is called the quality parameter.<sup>33</sup> As  $m$  gets smaller the maser will oscillate with less flux.] Filling factors ( $\eta'$ ) were calculated assuming that there was no distortion of the fields by the bulb; the spin-exchange cross section was assumed to be the same as that for hydrogen.<sup>11</sup> In Fig. 8, the places where the power output is zero indicate threshold fluxes for various maser parameters. In practice, measured threshold fluxes and values of  $\tau_2$  agreed quite well with those predicted by the computer program.

#### H. Spin-Exchange Limit

For the D maser as in the H maser, spin-exchange collisions allow one to broaden the atomic linewidth and thereby obtain a method of "tuning."<sup>11</sup> Spin-exchange collisions also play another important role in the D maser: If state selection is "ideal," then the oscillation on the  $6 \rightarrow 2$  transition tends to be maintained when the density of atoms increases rather than reduced as for the hydrogen  $\sigma$  maser. This behavior is analogous to that of the  $1 \rightarrow 4$  transition in the H maser.<sup>5,34</sup>

The above effect occurs because spin-exchange collisions conserve the  $z$  component of the total angular momentum  $\alpha(D)$  [ $\alpha(D) \equiv \langle F_z \rangle$ ]. It is most evident when all non-spin-exchange processes can be neglected (including radiation). In this case Eqs. (4.28) yield the equilibrium values<sup>5</sup>

$$D_{ii} = \frac{1}{2} \frac{(1 - P^2)^{3/2}}{3 + P^2} \left( \frac{1 + P}{1 - P} \right)^{M F_i}, \quad (4.29)$$

where  $P$  is the electron polarization ( $P \equiv 2\langle J_z \rangle$ ). For the beam entering the bulb (assuming ideal state selection),  $\alpha(D) = 0.5$ , and this value must be the same in the spin-exchange limit. Therefore we can use Eq. (4.29) and the expression for  $\alpha(D)$  in terms of the  $D_{ii}$  to find the  $D_{ii}$  in the spin-exchange limit. In particular, we find  $D_{22} - D_{66} \approx +0.087 \approx -(D_{33} - D_{55})$ . Therefore, when spin-exchange processes are important, the population difference  $D_{22} - D_{66}$  tends toward a positive value which maintains the  $2 \rightarrow 6$  oscillation while  $D_{33} - D_{55}$  tends toward a negative value which diminishes the radiation on the  $3 \rightarrow 5$  transition.

This is important because if spin-exchange relaxation could be neglected, then with "ideal" state selection both the  $2 \rightarrow 6$  and  $3 \rightarrow 5$  transition would radiate about equally. (The separation of the lines is much less than the cavity bandwidth.) This would cause the additional problem that the radiation from the  $3 \rightarrow 5$  transition would tend to pull the  $2 \rightarrow 6$

transition frequency.<sup>35</sup> Therefore it is desirable to work at flux levels where for a proper choice of cavity  $Q$ , the  $2 \rightarrow 6$  transition will oscillate but the  $3 \rightarrow 5$  transition will not.

The above behavior is observed in practice. At high-cavity  $Q$  and low fluxes (where spin-exchange relaxation is negligible) both transitions oscillate with about equal strength. As the  $Q$  is reduced, both oscillations die out at approximately the same point. At fluxes where spin exchange contributes to the atomic linewidth both transitions will oscillate at high-cavity  $Q$  but the  $3 \rightarrow 5$  oscillation has less strength. As the  $Q$  is reduced the  $3 \rightarrow 5$  oscillation dies out but the  $2 \rightarrow 6$  oscillation remains.

#### J. Solution for Oscillation Frequency

More important than an exact description of the power output of the maser is an accurate expression for the frequency of oscillation  $\nu(D)$ . Equation (4.20) relates this frequency to (i) the cavity (frequency and  $Q$ ) and (ii) the total atomic magnetization. Combining Eqs. (4.13), (4.23)–(4.25), and (4.26), using the approximations  $|\omega - \omega'_{62}| \ll \tau_2$ ,  $|\omega - \omega_{53}| \gg \tau_2$ , and noting that  $\langle 5 | J_x | 3 \rangle = -\langle 6 | J_x | 2 \rangle$  we can write the imaginary part of Eq. (4.20) in the form

$$\tau_2(\omega - \omega'_{62}) = Q_L \left( \frac{\omega_c}{\omega} - \frac{\omega}{\omega_c} \right) - \frac{D_{33} - D_{55}}{D_{22} - D_{66}} \tau_2^{-1} (\omega - \omega_{53})^{-1}. \quad (4.30)$$

This result is the same as that obtained for the hydrogen  $\sigma$  maser<sup>33</sup> except for the second term on the right-hand side, which represents the pulling of the  $2 \rightarrow 6$  transition by the  $3 \rightarrow 5$  transition.

A more intuitive way to obtain Eq. (4.30) is by the "phase-shift method." If we think in terms of the equivalent circuit model for the cavity (Fig. 7) we can make the following argument. The oscillating field induces a magnetization whose phase (given by the ac susceptibility) is  $\phi_{H-M}$  with respect to the field. This magnetization induces a "cavity voltage" given by  $V(M) = -K(d/dt)4\pi\eta'\langle M_x \rangle_b$  whose phase is  $\phi_{M-V(M)}$  with respect to the magnetization. This voltage induces a current ( $I$ ) in the cavity whose phase (derived from the series impedance of the equivalent circuit) is  $\phi_{V(M)-I}$  with respect to the voltage. This current gives rise to an oscillating magnetic field which by Ampère's law is in phase with the current. If we require consistency around the "loop" we must have

$$\phi_{H-M} + \phi_{M-V(M)} + \phi_{V(M)-I} = m(2\pi), \quad m = 0, 1, 2, \dots$$

It is straightforward to obtain expressions for the various phases and when this is done<sup>22</sup> we arrive at Eq. (4.30).

It should also be noted that the last term in Eq.

(4.30) could be obtained by approaching the problem in a slightly different way. Other authors<sup>10,36</sup> have considered that the presence of neighboring transitions causes a change in the permeability of the cavity which causes frequency shifts in the cavity and therefore in the maser. Both approaches are essentially the same. However, the one given here has the simplicity that the frequency of oscillation appears as a function of only two things: the empty cavity and the total magnetization. When the total magnetization is examined in detail this frequency shift appears straightforwardly.

#### V. FREQUENCY SHIFTS AND MEASUREMENT TECHNIQUE

The measurement procedure was essentially the same as that used in previous experiments with the hydrogen maser.<sup>7,37</sup> Therefore the following discussion will primarily concern the corrections that must be made to the D-maser frequency; the corrections that must be made to the H-maser frequency have been discussed elsewhere.<sup>7,10</sup>

In order to find  $\nu_0(D)$  we must correct the observed frequency  $\nu(D)$  for various frequency shifts which we group into five categories. Each of these categories is discussed below along with the accompanying measurement technique.

##### A. Cavity and Spin-Exchange Shifts; "Tuning" Procedure

The "tuning" procedure outlined in Ref. 11 provides a method for correcting the observed frequency for cavity and spin-exchange shifts thereby yielding  $\nu_{62}(D)$  (see Sec. IV D). It is valid if we can relate  $\nu_{62}(D)$  to the maser frequency  $\nu(D)$  by an equation of the form

$$\nu(D) - \nu_{62}(D) = (1/\tau_2) \{ K_c [\nu_c - \nu_{62}(D)] + K_{SE} \}, \quad (5.1)$$

where  $\nu_c$  is the cavity frequency,  $K_c$  is a constant depending on cavity parameters, and  $K_{SE}$  is a constant depending on spin-exchange parameters (but independent of  $\tau_2$ ). For the D maser Eq. (5.1) is not strictly true and is modified by the pulling due to the  $3 \rightarrow 5$  transition. By combining Eqs. (4.27) and (4.30), using the definitions for  $\omega'_{62}$ ,  $\Delta\omega_{62}(SE)$ , and  $I_0$ , and making the approximations that  $2Q_c \times (\omega_c - \omega_{62})/\omega_{62} \ll 1$  and  $Q_c/Q_a \ll 1$  ( $Q_a \equiv \nu_0 \pi \tau_2$ ) we obtain

$$\begin{aligned} 2\pi[\nu(D) - \nu_{62}(D)] &= \frac{1}{\tau_2} \left( \frac{2Q_c}{\nu_{62}(D)} [\nu_c - \nu_{62}(D)] - \frac{\kappa_{DD} m}{144 \langle 6 | J_x | 2 \rangle^2} \right) \\ &\quad - \left[ \frac{D_{33} - D_{55}}{D_{22} - D_{66}} \right] \{ 2\pi\tau_2^2 [\nu_{62}(D) - \nu_{53}(D)] \}^{-1}. \end{aligned} \quad (5.2)$$

Equation (5.2) has the form of Eq. (5.1) except for the last term, which accounts for the pulling of the  $3 \rightarrow 5$  transition. If we include this last term, then

in the terminology of Ref. 11 we can write

$$\nu(D)_B - \nu_{62}(D) = [\nu(D)_A - \nu(D)_B] / (R - 1) + \delta\nu_{53}(D), \quad (5.3)$$

where the subscripts *A* and *B* refer to the "high" - and "low" - flux conditions of the source (high- and low-atom-density configurations of the maser), and  $R \equiv \Delta\nu_{aA} / \Delta\nu_{aB}$  is the ratio of atomic linewidths for the *A* and *B* flux conditions. The quantities  $\nu(D)_A$ ,  $\nu(D)_B$ , and *R* are measured and  $\delta\nu_{53}(D)$  can be calculated (Sec. VE). Therefore we have a method of obtaining  $\nu_{62}(D)$ . We can now determine  $\nu_0(D)$  from the equation

$$\nu_{62}(D) = \nu_0(D) + \delta\nu_w(D) + \delta\nu_m(D) + \delta\nu_D(D), \quad (5.4)$$

where  $\delta\nu_w(D)$ ,  $\delta\nu_m(D)$ , and  $\delta\nu_D(D)$  are the wall, magnetic field, and second-order Doppler-shift corrections, respectively.

#### B. "Wall" Frequency Shift

The D-maser wall shift was measured by the deformable bulb technique.<sup>38,39</sup> That is, it could be derived by measuring the change in wall shift between the two volume configurations of the storage bulb and calculating the respective mean free paths ( $\lambda$ ) for atoms in the bulb. We have<sup>38,39</sup>

$$\delta\nu_w(D)_{1v} = \frac{\delta\nu_w(D)_{sv} - \delta\nu_w(D)_{lv}}{\lambda_{1v}/\lambda_{sv} - 1}, \quad (5.5)$$

where the subscripts *sv* and *lv* denote the small- and large-volume configurations of the storage bulb, respectively. For the D maser  $\lambda_{1v}/\lambda_{sv} = 1.255(10)$ , where the error is due to nonuniformities in the bulb contour. (The "stem" correction<sup>40</sup> was negligible.) It is perhaps more instructive to write Eq. (5.5) in the form

$$\delta\nu_w(D)_{1v} = \frac{[\nu_0(D) + \delta\nu_w(D)_{sv}] - [\nu_0(D) + \delta\nu_w(D)_{lv}]}{\lambda_{1v}/\lambda_{sv} - 1}. \quad (5.6)$$

Since  $\lambda_{1v}/\lambda_{sv} - 1$  is less than 1, this equation tells us that the largest error in the deuterium frequency is necessarily the error in our determination of  $\delta\nu_w(D)_{1v}$ . That is, the uncertainty in  $\delta\nu_w(D)_{1v}$  due to the uncertainty in  $\lambda_{1v}/\lambda_{sv}$  was in practice negligible and, therefore, the main uncertainty was due to the uncertainty in the relative determination of  $\nu_0(D) + \delta\nu_w(D)$  at the two volume configurations.

The H-maser wall shift was taken relative to that of Harvard Maser No. 1, whose wall shift has been measured several times.<sup>39,40,41</sup> Its uncertainty was taken as  $\pm 2.5 \times 10^{-3}$  Hz which accounts for the uncertainty in  $\nu_0(H)$ . Note however that this error does not contribute to the error in  $\delta\nu_w(D)$  because the hydrogen-maser wall shift, although not precisely known, was assumed to be constant for all measurements (see Sec. VIA).

#### C. Magnetic-Field Frequency Shift

As for the H maser<sup>10</sup> the magnetic field was monitored by inducing Zeeman transitions between the magnetic sublevels and observing the resonances by monitoring the power output of the maser. We want to set the magnetic field equal to the "field-independent" value; therefore the Breit-Rabi formula gives the relevant Zeeman frequencies ( $\nu_{z0}$ ) as

$$\nu_{z0}(2 \rightarrow 1) = 28\,600.2 \text{ Hz},$$

$$\nu_{z0}(2 \rightarrow 3) = 28\,605.2 \text{ Hz},$$

$$\nu_{z0}(6 \rightarrow 5) = 28\,645.3 \text{ Hz}.$$

When we are near the "field-independent" point, then

$$\delta\nu_m(D) = -10.01153 \left[ 1 - \left( \frac{\nu_z - \nu_{z0}}{\nu_{z0}} \right)^2 \right] \text{ Hz}. \quad (5.7)$$

#### D. Second-Order Doppler Shift

From Ref. 10,

$$\delta\nu_D(D)/\nu_0(D) = -0.689 \times 10^{-13} T, \quad (5.8)$$

where *T* is the temperature expressed in degrees Kelvin. The temperature was monitored by mercury thermometers placed inside the magnetic shields. From Eq. (5.6) we note that the relative calibration of the thermometers is more important than the absolute calibration.

#### E. Frequency Shift Caused by 3 $\leftrightarrow$ 5 Hyperfine Transition

Here we are interested in two things: (i) the shift  $\delta\nu_{53}(D)$  for each volume configuration of the storage bulb and (ii) the relative shift  $\delta\nu_{53}(D)_{sv} - \delta\nu_{53}(D)_{lv}$  for use in Eq. (5.6). In the notation of Sec. VA we have

$$\delta\nu_{53}(D) = (R\delta\nu_B^* - \delta\nu_A^*) / (R - 1), \quad (5.9)$$

where we have defined

$$\delta\nu^* \equiv - [2\pi\tau_2^2(\omega_{62} - \omega_{53})]^{-1} \left( \frac{D_{33} - D_{55}}{D_{22} - D_{66}} \right).$$

To get an idea of the magnitude of  $\delta\nu^*$  we write

$$\delta\nu^* \approx \frac{0.64}{\tau_2^2} \left( \frac{D_{33} - D_{55}}{D_{22} - D_{66}} \right) \times 10^{-3} \text{ Hz}.$$

Now  $\tau_2 \approx 1$  sec and  $(D_{33} - D_{55}) / (D_{22} - D_{66}) < 1$  (or else the 3 $\leftrightarrow$ 5 transition would oscillate) and therefore  $\delta\nu^* \lesssim 0.5 \times 10^{-3}$  Hz. Unfortunately a simple method does not exist for determining  $\delta\nu_{53}(D)$ . However the computer program discussed in Sec. IV G can be used to calculate  $\delta\nu^*$  [and  $\delta\nu_{53}(D)$ ] if the maser parameters ( $T_b$ , *m*, *R*,  $T_1$ ,  $T_2$ ,  $\tau_2$ ) are known. Plots of  $\delta\nu^*$  vs flux for various typical input parameters are shown in Fig. 9. If we know the value of  $\tau_2(B)$  for a particular set of input parameters, then

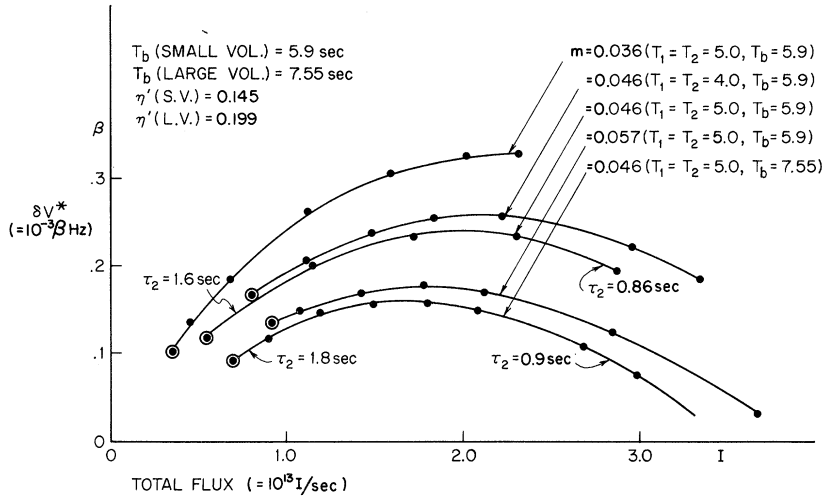


FIG. 9. Theoretical plots of  $\delta\nu^*$  vs atom flux.  $\odot$  denotes threshold flux.

the value of  $R$  yields  $\tau_2(A)$ . The computer program relates  $\tau_2$  to the flux and as indicated in Fig. 9 we can then relate particular values of  $\tau_2$  to the shift  $\delta\nu^*$ . In practice  $T_b$ ,  $m$ , and  $R$  were fairly well known while  $T_1$ ,  $T_2$ , and  $\tau_2$  were harder to determine (see Sec. VIB). If various possible combinations of input parameters are used (determined by the uncertainties in these parameters) then with the help of plots like those given in Fig. 9 we can obtain estimates of  $\delta\nu_{53}(D)$ . Such estimates yielded  $\delta\nu_{53}(D)_{1V} = (+0.1 \pm 0.3) \times 10^{-3}$  Hz for the data measurements. The error quoted here results from (i) the uncertainty of input parameters for a particular run and (ii) slight variations of input parameters over all the runs. Similarly we obtain

$$\delta\nu_{53}(D)_{sv} - \delta\nu_{53}(D)_{1V} = (+0.4 \pm 2.0) \times 10^{-4} \text{ Hz}.$$

#### F. Measurement Procedure

In taking data, it was necessary to overcome short-term fluctuations and compensate for drifts. (The main drift was that in the D-maser frequency caused by cavity temperature drifts.) In a time of about 2 h a "run" could be made consisting of a set of individual measurements of  $\nu_0(D) + \delta\nu_w(D) + \delta\nu_{53}(D)$ . Each run was made at one volume position of the deuterium storage bulb; changing the volume required letting the system rise to atmospheric pressure and pumping down again, which took about 3 days. Individual measurements were taken in the following manner.

(a) Both maser output frequencies were first tuned as well as possible to the resonant frequency of the atoms. This was done by observing the change in output frequencies for the  $A$  and  $B$  flux conditions and varying the cavity frequency to get a null result. (b) The D-maser magnetic field was adjusted to the "field-independent point" and then the H-maser Zeeman frequency was measured. (c) Three

10-sec averages of  $\nu_{\text{beat}}$  (the frequency at the counter in Fig. 6, which is typically  $\approx 1$  Hz) were made for the following configurations of the masers:  $H_A, D_B$ ;  $H_B, D_B$ ;  $H_B, D_A$ ;  $H_B, D_B$ ; and  $H_A, D_B$ , where  $H_A, D_B$  denotes that the H maser was in configuration  $A$  while the D maser was in configuration  $B$ , etc. Between measurements of  $\nu_{\text{beat}}$  for each of these configurations, it was necessary to wait for flux and amplitude levels to stabilize. Therefore, the relative times when  $\nu_{\text{beat}}$  was measured were recorded so that linear drifts could be compensated. (d) The Zeeman frequencies were remeasured to check for drifts.

Before and after each run the  $R$  ratios, the absolute temperatures, and  $\tau_2$  for the D maser were measured. Consistency was found in these measurements and therefore it was assumed these parameters were constant in a run.

## VI. RESULTS

### A. Frequency-Comparison Measurements

The results of the frequency-comparison measurements are displayed in Fig. 10. In Fig. 10 are plotted the average values of  $Y$  for each run (set of measurements of  $Y$ ) where  $Y$  is defined by

$$Y \equiv \nu_0(D) + \delta\nu_w(D) + \delta\nu_{53}(D) - 327\,384\,352.5100 \text{ Hz}. \quad (6.1)$$

Experimentally  $Y$  is determined from measurements of  $\nu_{\text{beat}}$  and the analysis of Secs. VA, VC, VD, and VE. Therefore, it is directly dependent on  $\nu_0(H)$ , which is assumed to be exactly 1420 405 751.768 Hz.<sup>41</sup> In the same way it is also dependent on  $\delta\nu_w(H)$  but at this point we neglect the uncertainty in  $\delta\nu_w(H)$  because  $\delta\nu_w(H)$  cancels out in our determination of  $\delta\nu_w(D)$  from measurements of  $Y$  for the two volume configurations of the D maser. Later of course we must include this error when we calculate  $\nu_0(D)$  from the definition of  $Y$ .

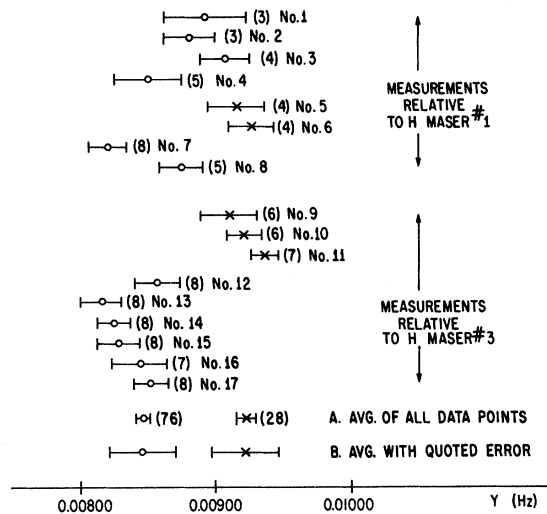


FIG. 10. Results of data runs. O, measurements at small volume; X, measurements at large volume; ( $n$ ) denotes number of data points in a particular run.

The error bars in Fig. 10 correspond to the deviation of the mean ( $\sigma_j$ ) for each run, which is defined by

$$\sigma_j^2 = \sum_{i=1}^{N_j} (Y_i - \bar{Y}_j)^2 / N_j(N_j - 1), \quad (6.2)$$

where  $\bar{Y}_j$  is the average value of  $Y$  for run  $j$ ,  $Y_i$  is the value of  $Y$  for measurement  $i$  in run  $j$ , and  $N_j$  is the number of measurements in run  $j$  (indicated beside the error bars for each run). These error bars corresponded only to the fluctuations between separate measurements of  $Y$  in a particular run; uncertainties in the frequency corrections  $\delta\nu_m(D)$ ,  $\delta\nu_D(D)$ ,  $\delta\nu_m(H)$ , and  $\delta\nu_D(H)$  were negligible compared to these fluctuations, and therefore they were assumed to be zero for each measurement of  $\bar{Y}$ .

In particular, rms fluctuations in measurements of  $\nu_{\text{beat}}$  over 10-sec averaging times were typically  $3.0 \times 10^{-4}$  Hz. [These fluctuations were predominantly caused by fluctuations in  $\nu(D)$ .] For both masers, uncertainties in the measurement of  $R$  could be neglected compared to this and therefore uncertainties in the calculation of cavity and spin-exchange shifts were due to fluctuations in  $\nu_{\text{beat}}$ . Fluctuations and drifts in the D-maser Zeeman frequencies over the measurement time were typically  $\lesssim 10$  Hz away from  $\nu_{\pi_0}$ ; therefore the uncertainty in the magnetic field frequency shift was negligible. It should be noted that the fluctuations in magnetic field were due to external magnetic perturbations and not to fluctuations in the solenoid current supply. This was consistent with the observation that magnetic fluctuations were greatly

reduced in late evening and early morning as opposed to daytime when there was activity in adjacent laboratories. Similarly, uncertainties in the Doppler-shift correction due to temperature fluctuations could be neglected. Fluctuations in maser parameters were small enough that fluctuations in  $\delta\nu_{53}(D)$  for measurements in a particular run could be neglected. Finally, uncertainties in the H-maser corrections  $\delta\nu_m(H)$  and  $\delta\nu_D(H)$  could also be neglected compared to fluctuations in  $\nu_{\text{beat}}$ .

In Fig. 10, the points labeled A correspond to  $\bar{Y} \pm \sigma$  for the entire collection of measurements at each volume. (Strictly speaking we should separately evaluate the data taken relative to H masers 1 and 3 because of calibration errors between them. These errors however could be neglected.) The data appear to exhibit nonstatistical fluctuations. This is reflected in the Birge ratio ( $R_B$ ),<sup>42</sup> which for the data at small volume is  $R_B \approx 1.8$ . This behavior could partly be explained by the small number of measurements in some of the runs. Systematic effects between runs could also cause these results; some of the more important of these effects are discussed in Sec. VII. However because this nonstatistical behavior could not be adequately explained, the errors on  $\bar{Y}$  for both volumes were increased to those indicated by the letter B in Fig. 10. That is,  $Y_{sv} = 0.00846(25)$  Hz;  $Y_{lv} = 0.00922(25)$  Hz.

Using the value of  $\delta\nu_{53}(D)_{sv} - \delta\nu_{53}(D)_{lv}$  from Sec. VE and applying Eq. (5.6) we obtain

$$\delta\nu_w(D)_{lv} = -0.0031(16) \text{ Hz.}$$

It is interesting to compare this result with that which we might expect assuming a value for  $\delta\phi$ , the phase shift per wall collision. Unfortunately, no wall-shift data exist for the FEP Teflon film used in this experiment. However for the hydrogen maser,  $\delta\phi$  has been measured for two different samples of DuPont FEP-120 Teflon film coated onto quartz storage bulbs.<sup>40,43</sup> These measurements indicated that for hydrogen at 22 °C we would expect

$$\delta\phi \equiv \delta\phi_{43}(H) \approx -9.6 \times 10^{-6} \text{ rad/collision (Ref. 43),}$$

$$\delta\phi \equiv \delta\phi_{40}(H) \approx -6.9 \times 10^{-6} \text{ rad/collision (Ref. 40).}$$

A theory of alkali-wall collisions<sup>44</sup> predicts that  $\delta\phi = f\nu_0 m^{1/2}$ , where  $m$  is the atomic mass,  $\nu_0$  is the atomic hyperfine frequency, and  $f$  depends on the surface and atoms but should be the same for the hydrogen isotopes. Therefore for deuterium on DuPont FEP-120 Teflon we would expect

$$\delta\phi_{43}(D) \approx -3.2 \times 10^{-6} \text{ rad/collision,}$$

$$\delta\phi_{40}(D) \approx -2.3 \times 10^{-6} \text{ rad/collision.}$$

If this type of Teflon were coated onto the D-maser

bulb ( $\lambda_{1\nu} \approx 14.7$  in.), then by Eq. (3) of Ref. 40 we should expect

$$\delta\nu_w(D)_{1\nu_{43}} \approx -0.0024 \text{ Hz},$$

$$\delta\nu_w(D)_{1\nu_{40}} \approx -0.0017 \text{ Hz}.$$

Since a 40% change was observed in the two different samples of the same kind of Teflon used in the hydrogen masers, the agreement of these estimates with the value measured in this experiment is probably good.

Including the H-maser wall-shift error we obtain  $Y_{1\nu} = 0.009\,22(63)$  Hz. Using the estimate of  $\delta\nu_{53}(D)_{1\nu}$ , Eq. (6.1) yields

$$\nu_0(D) = 327\,384\,352.5222(17) \text{ Hz}.$$

This value of  $\nu_0(D)$  agrees with but is more accurate than an earlier determination by Larson,<sup>2</sup> who obtained

$$\nu_0(D) = 327\,384\,352.51(5) \text{ Hz}.$$

It should be noted that the error quoted in the present experiment is a factor of 3 larger than would be obtained if the dominant error in the experiment was that due to the H-maser wall-shift uncertainty.

#### B. Measurement of Decay Rates

Measurements of  $\tau_2$  could be made<sup>10</sup> by using the pulsing scheme discussed in Sec. III D. In practice it was necessary from the standpoint of  $S/N$  to operate at flux levels where spin-exchange collisions contributed to the linewidth. Therefore, it was difficult to separate  $T_2$  from  $\tau_2$ , and measurements indicated only that  $T_2 \gtrsim 3.2$  sec. Field-inhomogeneity relaxation was negligible and therefore it was assumed that  $T_2 \approx T_{2w}$ . This can be compared with the range of possible expected values of  $T_{2w}$  given in Sec. III A.

### VII. SYSTEMATIC FREQUENCY SHIFTS

It is useful to divide possible systematic frequency shifts into two categories: (i) Systematic shifts that occur in the known frequency corrections due to improper measurement techniques. For instance, we might ask if the magnetic field changes when we go from configuration  $B$  to configuration  $A$  in the D maser. If it does, then we introduce an error in our calculations of  $\nu_0(D)$  because we measure  $\nu_z(D)$  for only one configuration and assume that it stays constant. (ii) Systematic shifts due to frequency corrections not accounted for in Sec. V.

#### A. Systematic Shifts in Known Frequency Corrections

It was possible to check for most effects of systematic shifts in the known frequency corrections. Some of the more important possible shifts are the following.

(a) Does changing the D maser from condition  $A$  to  $B$  change its cavity frequency? This type of ef-

fect might arise if for instance the gain of the feedback amplifier was nonlinear [see Eq. (A1)]. The most rigorous test of this effect was to study Eq. (5.2) for a range of atom fluxes. Tests were made by operating the maser in three flux conditions for which the ratios of the atomic linewidths were known. Including the effects of the pulling by the 3—5 transition, agreement with Eq. (5.2) (where  $\nu_c$  is assumed constant) was obtained.

(b) Is  $\delta\nu_{53}(D)$  constant for all the runs? Because maser parameters varied slightly over the various runs,  $\delta\nu_{53}(D)$  could not be held constant. However, with the help of the computer program it was estimated that upper limits on the variation of  $\delta\nu_{53}(D)$  over the entire set of runs was  $\pm 0.15 \times 10^{-3}$  Hz, which is not large enough to explain the nonstatistical fluctuations.

(c) Does changing the bulb volume change the bulb surface? Here we encounter the most serious objection to the deformable bulb technique<sup>38,39</sup> for measuring the wall shift. Such an effect would probably be small because the total wall shift is small and the amount of flexing of the bulb surface is rather small. Large effects would also give anomalous relaxations.

The D maser reported here had an additional disadvantage, namely, provision was not made for changing the storage bulb volume under vacuum. This meant that between runs at the small- and large-volume configuration, the bulb surface was exposed to air and perhaps contamination which might result in a changing surface. Although the presence of such contamination could not easily be detected, the result of Sec. VII B (c) gave some indication that it did not cause large effects.

#### B. Other Systematic Shifts

Several possibilities of other systematic shifts were investigated, of which some of the more important are the following.

(a) First-order Doppler shift. Theoretically such a shift would be negligible; a partial test for such a shift is provided by measurements of  $Y$  with the input and output lines to the cavity reversed. A null result was found.

(b) Corrections to spin-exchange equations caused by nuclear identity. In Sec. IV A, Eqs. (4.2)–(4.4) were derived assuming that the nuclei of the deuterium atoms in a collision are distinguishable. Crampton<sup>26</sup> has outlined the procedure for taking their indistinguishability into account and when this is done<sup>22</sup> the pulling due to spin exchange [Eq. (5.2)] is no longer strictly proportional to  $\tau_2^{-1}$ . However estimates of the magnitude of this correction<sup>22</sup> indicated that it is negligible here.

(c) Corrections to spin-exchange equations caused by a wall-polarization effect. A wall-polarization effect has been used to account for relaxation and

frequency shifts in maser storage bulbs.<sup>4,13,23</sup> The basic mechanism for this shift has been discussed elsewhere.<sup>4,45</sup> It can arise in transitions where the average value of the electron spin changes, and it is proportional to the collision rate with polarized spin sites on the wall. Larson<sup>4</sup> could explain a shift in his measurements by the above effect. If we assume that the D-maser storage bulb surface was the same as that in Larson's H maser, then we would expect a wall-polarization shift in the D maser of  $\approx 0.016 \times 10^{-3}$  Hz.<sup>22</sup> If the D-maser bulb had significantly more spin sites on the wall, one might expect difficulties. One means for studying this effect was to change the temperature of the bulb and see if any shift could be observed. (Larson observed a 100% change in making measurements at 27 and 40 °C.) Therefore, relative measurements of  $Y$  were made at 20.8 and 30.8 °C. The difference was  $|\Delta Y| = (0.16 \pm 0.26) \times 10^{-3}$  Hz.

(d) Inhomogeneity shifts due to quadratic averaging. In this case we are interested in a shift expressed as

$$\delta\nu_{I_1} = \langle \nu(H_0) \rangle - \nu(\langle H_0 \rangle),$$

where  $H_0$  is the external magnetic field and the brackets denote the volume average over the storage bulb. Neglecting the shift discussed in Sec. VII B(e),  $\langle \nu(H_0) \rangle$  is the output frequency of the maser and  $\nu(\langle H_0 \rangle)$  is the calculated output frequency using the value of  $\langle H_0 \rangle$  inferred from the Zeeman frequency measurements. If we choose a simple model for the magnetic field inhomogeneity, then we can relate the dephasing relaxation to the inhomogeneity<sup>10</sup> and therefore to the shift  $\delta\nu_{I_1}$ . Such estimates based on magnetic-linewidth studies<sup>22</sup> indicated that this shift was negligible for both masers.

(e) Inhomogeneity shift due to poor volume averaging. Brenner has discovered an inhomogeneity frequency shift that can arise in motional averaging systems.<sup>46</sup> This shift can in general be expressed as

$$\delta\nu_{I_2} = \nu_{\text{obs}} - \langle \nu(H_0) \rangle,$$

where  $\nu_{\text{obs}}$  is the observed frequency. Such a shift can occur if the volume to which the atoms are confined is composed of two poorly communicating subregions that have different average values of magnetic field and consequently different average frequencies. In the maser, the bulb and bulb-collimating stem are in this category of subregions and shifts of this type have been observed.<sup>46</sup>

These shifts however are more likely to occur on strongly field-dependent lines rather than the highly field-independent lines used in this experiment. Using Brenner's theory and estimates of possible field inhomogeneities as in Sec. VII B(d) such shifts would be negligible for both masers. In the D maser, they could experimentally be ruled out by

calibrating the average magnetic field with transitions of different field dependence.<sup>4</sup> If consistency is found then the Brenner shift could be ruled out. In particular, for the D maser, the field could be calibrated by observing Zeeman transitions (proportional to electron moment) and also by observing the difference frequency between the 6 → 2 and 5 → 3 transitions (proportional to the nuclear moment). Agreement was found and from this result, the Brenner shift was totally negligible.

#### VIII. D MASER AS FREQUENCY STANDARD

One might consider the use of the D maser as a frequency standard. Although the performance of the device reported here was not as good as the H maser, the authors think that the experiment could be improved by (i) making a provision for changing the bulb volume under vacuum and (ii) increasing  $\tau_2$  and thereby reducing  $\delta\nu_{53}(D)$ . As a primary standard the D maser has the advantage that its fractional wall shift ( $\delta\nu_w/\nu_0$ ) is smaller than in the hydrogen maser by the ratio of mean free paths of atoms in the bulb. (Of course the multiple-region hydrogen maser<sup>15</sup> is better than the D maser in this respect.) It appears however to be limited by (i) the pulling of the 5 → 3 transition and (ii) the effect of nuclear identity on spin-exchange shifts (Sec. VII B), both of which add systematic corrections to Eq. (5.1) that are difficult to calculate. The hydrogen maser is free of the above difficulties, and therefore appears to be superior as a primary standard.

#### IX. GRAVITATIONAL DIPOLE MOMENT IN THE DEUTERON

A few authors<sup>47</sup> have discussed the theoretical possibilities for a nuclear particle possessing a gravitational dipole moment. Velyukhov<sup>48</sup> claimed that he had found evidence for a gravitational dipole moment in the proton. Subsequent measurements were made<sup>49</sup> that invalidated this earlier measurement; Young<sup>50</sup> established an upper limit of 0.3 Hz on the gravity shift of the proton Larmor frequency.

If the deuteron possesses a gravitational dipole moment  $\xi_D \vec{I}$ , then we must add the term  $-\xi_D \vec{I} \cdot \vec{g}$  to the Hamiltonian of Eq. (2.1) ( $\vec{g}$  is the acceleration of gravity in the laboratory). For the 2 → 6 transition,  $\Delta I_z \approx 1$ ,  $\Delta J_z \approx 0$ . We would evidently see a shift of  $2\xi_D g h^{-1}$  Hz between measurements of  $Y$  with the gravitational and magnetic fields parallel or antiparallel. Such measurements were easily made with the present apparatus, and an upper limit could be established on the gravity shift of the deuteron Larmor frequency. We found  $\xi_D g h^{-1} < 10^{-4}$  Hz.

If we write  $\xi_D$  in units of proton mass and Fermi length, the above result indicates that  $\xi_D < 3000$  proton-F. From the equivalence principle  $\xi_D$  should be zero; moreover one might not expect to see an effect until  $\xi_D$  was measured to less than 1 proton-F.

## ACKNOWLEDGMENTS

The authors wish to thank the other members of the hydrogen-maser and molecular-beam groups at Harvard for their help throughout the course of this work; in particular D. Larson provided many useful discussions. We thank V. Reinhardt for the computer program used to solve the equations of motion and F. Robie for help in cavity design.

## APPENDIX A: CAVITY WITH FEEDBACK

For the problem of a cavity with feedback, the circuit analog for the maser (Sec. IV F) is especially useful. We assume that we can represent the feedback network (Fig. 5) by a single amplifier with input impedance  $R_L$ , output impedance  $R_G$ , and voltage gain  $A = A_0 e^{i\theta}$ , where  $\theta$  is the total phase shift in the feedback loop. Then the circuit analog for the maser can be given as in Fig. 11. We can solve the circuit problem for the effective series impedance seen by the magnetization voltage

$$V_m = -K \frac{d}{dt} 4\pi\eta' \langle M_x \rangle_b,$$

and we obtain (assuming for simplicity  $R_L = R_G = Z_0$ )

$$V_m/I = Z_{\text{eff}} = R[1 + \beta_1 + \beta_2 - A_0(\beta_1\beta_2)^{1/2} \cos\theta]$$

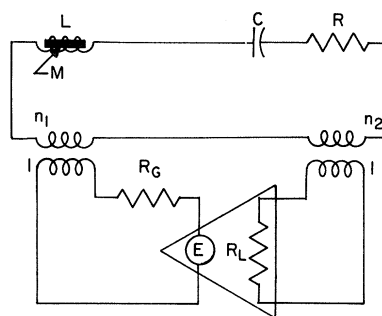


FIG. 11. Model of cavity with feedback network.

$$+ iR[Q_0(\nu/\nu_c - \nu_c/\nu) - A_0(\beta_1\beta_2)^{1/2} \sin\theta], \quad (\text{A1})$$

where

$$\beta_1 = n_1^2 Z_0 R^{-1}, \quad \beta_2 = n_2^2 Z_0 R^{-1}, \quad Q_0 = 2\pi\nu_c LR^{-1}.$$

If we assume  $\theta = \theta_0 + a_1(\nu - \nu_c)$  and make the approximations that  $(\nu - \nu_c)/\nu_c \ll 1$  and  $\theta \ll 1$ , then  $Z_{\text{eff}}$  can be written in the form

$$Z_{\text{eff}} = R' [1 + iQ'' 2(\nu - \nu_c')/\nu_c'] .$$

This expression has the same form as the series impedance (near resonance) of a cavity without feedback.

\*Work supported by the Office of Naval Research.

†National Science Foundation Graduate Fellow.

‡Present Address: Physics Department, University of Washington, Seattle, Wash. 98105.

<sup>1</sup>F. Low and E. Salpeter, *Phys. Rev.* **83**, 478 (1951).

<sup>2</sup>D. J. Larson, P. A. Valberg, and N. F. Ramsey, *Phys. Rev. Letters* **23**, 1369 (1969).

<sup>3</sup>W. M. Hughes and H. G. Robinson, *Phys. Rev. Letters* **23**, 1209 (1969).

<sup>4</sup>D. J. Larson, thesis (Harvard University, 1970) (unpublished).

<sup>5</sup>S. B. Crampton, H. G. Robinson, D. Kleppner, and N. F. Ramsey, *Phys. Rev.* **141**, 55 (1966).

<sup>6</sup>G. S. Hayne, E. S. Ensberg, and H. G. Robinson, *Phys. Rev.* **171**, 20 (1968).

<sup>7</sup>S. B. Crampton, D. Kleppner, and N. F. Ramsey, *Phys. Rev. Letters* **11**, 338 (1963).

<sup>8</sup>G. Breit and I. I. Rabi, *Phys. Rev.* **38**, 2082 (1931).

<sup>9</sup>N. F. Ramsey, *Molecular Beams* (Oxford U.P., New York, 1956).

<sup>10</sup>D. Kleppner, H. M. Goldenberg, and N. F. Ramsey, *Phys. Rev.* **126**, 603 (1962).

<sup>11</sup>D. Kleppner, H. C. Berg, S. B. Crampton, N. F. Ramsey, R. F. Vessot, H. E. Peters, and J. Vanier, *Phys. Rev.* **138**, A972 (1965).

<sup>12</sup>N. F. Ramsey, *Am. Scientist* **56**, 420 (1968).

<sup>13</sup>H. C. Berg, *Phys. Rev.* **137**, A1621 (1965).

<sup>14</sup>R. Vessot, M. Levine, L. Cutler, M. Baker, and L. Mueller, in *Proceedings of the Twenty-Second Annual Symposium on Frequency Control* (U.S. Army Electronics Command, Ft. Monmouth, N. J., 1968), p. 605.

<sup>15</sup>E. E. Uzgiris and N. F. Ramsey, *Phys. Rev. A* **1**, 429 (1970).

<sup>16</sup>E. E. Uzgiris, thesis (Harvard University, 1968) (unpublished).

<sup>17</sup>P. W. Zitzewitz, thesis (Harvard University, 1970) (unpublished).

<sup>18</sup>DuPont FEP type-A Teflon film.

<sup>19</sup>Precision Coating, Dedham, Mass.

<sup>20</sup>It is assumed that the relaxation probability per collision is the same for deuterium and hydrogen.

<sup>21</sup>H. Hellwig and E. Pannaci, *J. Appl. Phys.* **39**, 5496 (1968); C. Audoin, *Compt. Rend.* **263**, 542 (1966); F. Hartman, *Phys. Letters* **24A**, 767 (1967).

<sup>22</sup>D. J. Wineland, thesis (Harvard University, 1970) (unpublished).

<sup>23</sup>H. C. Berg, thesis (Harvard University, 1964) (unpublished).

<sup>24</sup>L. C. Balling, R. J. Hanson, and F. M. Pipkin, *Phys. Rev.* **133**, A607 (1964).

<sup>25</sup>P. L. Bender, *Phys. Rev.* **132**, 2154 (1963).

<sup>26</sup>S. B. Crampton, thesis (Harvard University, 1964) (unpublished).

<sup>27</sup>The distinction to be made is that self-sustained oscillations do not occur on the  $3 \leftrightarrow 5$  transition. However it radiates slightly because it is driven (nonresonantly) by the  $6 \leftrightarrow 2$  radiation.

<sup>28</sup>J. H. Shirley, *Am. J. Phys.* **36**, 949 (1968).

<sup>29</sup>W. H. Louisell, *Radiation and Noise in Quantum Electronics* (McGraw-Hill, New York, 1964).

<sup>30</sup>J. C. Slater, *Rev. Mod. Phys.* **18**, 441 (1946).

<sup>31</sup>In more complicated systems this is a convenience. See, for example, Ref. 15.

<sup>32</sup>A. E. Siegman, *Microwave Solid State Masers* (McGraw-Hill, New York, 1964); E. L. Ginzton, *Microwave Measurements* (McGraw-Hill, New York, 1957); N. N.

- Beringer, MIT Rad. Lab. Series 11 (1964).
- <sup>33</sup>S. B. Crampton, Phys. Rev. 158, 57 (1967).
- <sup>34</sup>P. A. Valberg and N. F. Ramsey, Phys. Rev. A 3, 554 (1971).
- <sup>35</sup>N. F. Ramsey, Phys. Rev. 100, 1191 (1955).
- <sup>36</sup>H. M. Goldenberg, thesis (Harvard University, 1960) (unpublished); K. Shimoda, T. C. Wang, and C. H. Townes, Phys. Rev. 102, 1308 (1956).
- <sup>37</sup>B. S. Mathur, S. B. Crampton, D. Kleppner, and N. F. Ramsey, Phys. Rev. 158, 14 (1967).
- <sup>38</sup>D. Brenner, Bull. Am. Phys. Soc. 14, 943 (1969).
- <sup>39</sup>P. E. Debely, Rev. Sci. Instr. 41, 1290 (1970).
- <sup>40</sup>P. W. Zitzewitz, E. E. Urgiris, and N. F. Ramsey, Rev. Sci. Instr. 41, 81 (1970).
- <sup>41</sup>H. Hellwig, R. F. C. Vessot, M. Levine, P. W. Zitzewitz, H. E. Peters, D. W. Allan, and D. J. Glaze, IEEE Trans. Instr. Meas. IM-19, 200 (1970).
- <sup>42</sup>B. N. Taylor, W. H. Parker, and D. N. Langenberg, Rev. Mod. Phys. 41, 375 (1969).
- <sup>43</sup>R. Vessot *et al.*, IEEE Trans. Instr. Meas. IM-15, 165 (1966).
- <sup>44</sup>M. Goldenberg, D. Kleppner, and N. F. Ramsey, Phys. Rev. 123, (1961).
- <sup>45</sup>P. A. Valberg, Phys. Rev. A 3, 505 (1971).
- <sup>46</sup>D. Brenner, thesis (Harvard University, 1968) (unpublished); Phys. Rev. 185, 26 (1969).
- <sup>47</sup>I. Yu. Kobzarev, L. B. Okun', Zh. Eksperim. i Teor. Fiz. 43, 1904 (1962) [Sov. Phys. JETP 16, 1343 (1963)]; L. B. Okun' and C. Rubbia, in *Proceedings of the International Conference on Elementary Particles, Heidelberg, 1967*, edited by H. Filthuta (North-Holland, Amsterdam, 1968), p. 338; I. Leitner and S. Okubo, Phys. Rev. 136B, 1542 (1964).
- <sup>48</sup>G. E. Velyukhov, Zh. Eksperim. i Teor. Fiz. Pis'ma v Redaktsiyu 8, 372 (1968); [Sov. Phys. JETP Letters 8, 229 (1968)].
- <sup>49</sup>B. V. Vasil'ev, Zh. Eksperim. i Teor. Fiz. Pis'ma v Redaktsiyu 9, 299 (1969) [Sov. Phys. JETP Letters 9, 175 (1969)].
- <sup>50</sup>B. A. Young, Phys. Rev. Letters 22, 1445 (1969).

## Spontaneous-Emission Profiles of Argon-Ion Laser Transitions\*<sup>†</sup>

R. C. Sze<sup>‡</sup> and W. R. Bennett, Jr.

*Dunham Laboratory, Yale University, New Haven, Connecticut 06520*

(Received 14 July 1971)

Experimental studies are reported of spontaneous-emission profiles observed in the axial and radial directions from high-current arc discharges of the type used in cw argon-ion lasers. The greatly increased sensitivity from a new computer-oriented method of line-profile analysis has permitted observation of linewidth parameters over a wide range of discharge current and pressure. These studies have shown the existence of several interesting new effects and have required a substantial modification of previously held concepts regarding the nature of line broadening in these discharges. A new theory for line-profile analysis in the radial direction is presented which incorporates the Tonks-Langmuir potentials and provides a correction for an arbitrary number of charge-exchange collisions in the radial acceleration of ions to the wall. A modification of the earlier theory of Kagan and Perel is suggested which brings that method of transverse line-profile analysis into reasonably close agreement with the present (more complex) method of analysis. Values for the mean radial velocity and electron temperature are obtained from profile analysis in the transverse direction. Studies of ion and neutral temperatures based on Voigt profile analysis in the axial direction are presented, along with the determination of the average electron density based on Stark broadening of the neutral and ionic lines. Precise values of the natural widths on the major argon-ion laser transitions are determined through extrapolations of the axially observed Lorentz-width data taken at low pressures to zero discharge current.

### I. INTRODUCTION

The interpretation of spontaneous-emission profiles from ion laser transitions in high-current arc discharges has been the subject of a number of recent papers.<sup>1-5</sup> Previous experimental studies have demonstrated the existence of many interesting and seemingly anomalous properties of these discharges: for example, strongly current-dependent broadening, lack of thermodynamic equilibrium of excited species, and strongly anisotropic velocity distributions of excited-state ions. The previously reported experimental studies of the problem were

conducted with relatively low-resolution spectroscopic techniques which were incapable of determining much more than the full linewidths involved. We have recently developed much more precise and sensitive methods for line-profile analysis which permit detailed scrutiny of the line shape, as well as the extraction of linewidth parameters, over a wide range of intensity.<sup>6</sup> Application of our present technique to the study of the argon-ion laser transition has shown that several major modifications of the previous assumptions on line shape are required for an adequate description of light emitted from the high-current low-pressure capillary discharges